

Article

Identification of Ratholes in Desert Steppe Based on UAV Hyperspectral Remote Sensing

Xinchao Gao, Yuge Bi and Jianmin Du *

College of Mechanical and Electrical Engineering, Inner Mongolia Agricultural University, Hohhot 010018, China
* Correspondence: nndjwc202@imau.edu.cn; Tel.: +86-1524-8113-428

Abstract: This paper established a mathematical method for the spectral feature extraction of ratholes, based on UAV hyperspectral imaging technology. The degradation of grasslands is a major challenge to terrestrial ecosystems. Rodents not only promote soil erosion and accelerate the process of grassland degradation, but also carry diseases that can easily cause epidemics. The calculation of the number of rodent holes and grassland vegetation cover is an important indicator for monitoring and evaluating grassland degradation. Manual surveys have drawbacks in efficiently monitoring large areas and are human- and material-costly, hardly meeting the current needs of grassland degradation monitoring. Therefore, there is an urgent need to conduct real-time dynamic monitoring of grassland rathole distributions and grassland degradation processes. In this study, a low-altitude remote sensing platform was constructed by integrating a hyperspectral imager with a UAV to collect spectral data of the desert steppes in central Inner Mongolia Autonomous Region, China. Then, the spectral features of ratholes were extracted via radiation correction, noise reduction, and principal component analysis (PCA). Meanwhile, the spectral features of vegetation and bare soil were extracted based on the normalized difference vegetation index (NDVI), which was inputted to calculate the vegetation cover. The results showed that the single-band map extracted based on PCA could effectively determine the location of ratholes, where the overall accuracy and kappa coefficient were 97% and 0.896, respectively. Therefore, the method proposed in this study can accurately identify the location of desert steppe rodent holes. It provides a high-precision technical means for scientific and effective control of grassland rodent infestation and also provides a higher technical means for grassland degradation.

Keywords: hyperspectral image; monitoring of grassland degradation; rathole recognition; principal component analysis



Citation: Gao, X.; Bi, Y.; Du, J. Identification of Ratholes in Desert Steppe Based on UAV Hyperspectral Remote Sensing. *Appl. Sci.* **2023**, *13*, 7057. <https://doi.org/10.3390/app13127057>

Academic Editors:
Samuel Adelabu,
Romano Lottering and
Kabir Peerbhay

Received: 9 May 2023
Revised: 2 June 2023
Accepted: 9 June 2023
Published: 12 June 2023



Copyright: © 2023 by the authors. Licensee MDPI, Basel, Switzerland. This article is an open access article distributed under the terms and conditions of the Creative Commons Attribution (CC BY) license (<https://creativecommons.org/licenses/by/4.0/>).

1. Introduction

Grassland ecosystems play a major role in regulating the process of climate change on Earth and are an important production base for the development of grassland livestock farming, as well as an important ecological barrier [1]. In recent years, grassland ecosystems have been destroyed to different degrees due to both natural and human factors [2,3]. Among them, grassland rodent infestation is an important cause of grassland ecosystem degradation. A large number of vermin occupy grassland resources, digging and making holes, resulting in a large reduction in the grassland area and a decrease in the livestock carrying capacity of grasslands, which has caused serious economic losses among herders. Pest rats belong to the rodent group. According to a previous survey, there are more than 2000 species of rodents worldwide, carrying about 200 species of pathogens, accounting for about 25% of the pathogens in humans [4]. Among dozens of rodent-borne diseases, plague, hemorrhagic fever with renal syndrome (HFRS), and leptospirosis are infectious diseases that are legally prevented in China, which pose a serious threat to human life and health safety [5].

China has one of the largest grassland areas in the world, with a natural grassland area of approximately 400 million hectares, accounting for 40% of its total land area and

roughly 13% of the world's total grassland area [6,7]. With a total grassland area of 88 million hectares, which accounts for 20.06% of the national grassland area, Inner Mongolia is the second largest province in China in terms of grassland area, and the largest in terms of pastoral area. A previous survey revealed that the grassland rodent pest area in the Inner Mongolia Autonomous Region covers 6.54 million hectares, with a severely affected area of 2.83 million hectares. The expansion of grassland rodent pest areas, coupled with the sharp increase in pest numbers, not only poses a significant threat to the ecological balance of grasslands, causing severe degradation, but also increases the risk of a plague outbreak.

Rapid and accurate positioning of the geographical coordinates of rodent holes, combined with real-time and dynamic monitoring of changes in their numbers and distribution, is a crucial method to contain the occurrence of rodent pests. Grassland degradation mainly consists of vegetation degradation as well as soil degradation. Vegetation degradation refers to the reduction in high-quality forage production and the decline in vegetation species. Soil degradation refers to the reduction in organic matter content and soil erosion. Soil degradation is the precondition for vegetation degradation, and vegetation degradation is the inevitable result of soil degradation. Pest rats destroy soil and gnaw pasture, which are important causes of grassland degradation. Therefore, investigating the number of grassland pest rodent holes is an important basic link to monitoring grassland degradation and assessing the degradation level. The number of ratholes as well as the geographical coordinates can be manually surveyed with high accuracy. Based on the sample scale (0.25~1 hectare), the hole coefficient of pest rats can be calculated, and the density of rats can be investigated by plugging holes and pinning lines. By observing whether there are signs of activity around the holes, researchers can effectively differentiate between active and abandoned holes [8]. However, manual surveys are not only time-consuming and labor-intensive, but also, in the event of rodent infestation, hindered by the risk of potential virus transmission, threatening the lives of investigators [9]. Satellite remote sensing is a useful tool for large-scale spatial investigations. By obtaining satellite data, vegetation index calculations can be performed to achieve the estimation of above-ground biomass [10,11]. However, satellite remote sensing is limited by the external environment and the accuracy of its own sensors, meaning it cannot meet human expectations for small-feature surveys, such as rathole surveys [12,13]. Manned aircraft, which are commonly used for low-altitude remote sensing, have limited flight altitudes due to their fixed-wing design, making it difficult to achieve low-altitude flight and meet the precision requirements for data collection. In summary, the data collection methods mentioned above that are based on the rapid location of rodent holes may involve some risk of data loss or omission during the data acquisition process. Nevertheless, they still offer some degree of feasibility for analysis in the context of rodent hole investigation.

Field surveys based on low-altitude UAV remote sensing platforms are of great interest and popularity. The main reasons are as follows: (1) they offer the ability to enter hazardous areas for surveying; (2) they represent a new cost-effective way to detect small-scale spaces; and (3) they have the advantages of speed, efficiency, and simplicity of operation. UAVs depend on their unique advantageous conditions to fill the gap in using low-altitude remote sensing platforms in the field of small-scale investigation. Hyperspectral images have multiple continuous bands, which can be used to obtain both high temporal and spatial resolutions of the spectral data. Each pixel and band in the image contains rich spectral feature information and spatial information, helping to truly achieve "spectrum integration" and effectively express the real information of the measured object. At present, low-altitude UAV remote sensing platforms with hyperspectral imagers are widely used in the dynamic monitoring of large-area data in, for example, agriculture and forestry, as well as in the recovery monitoring of mining areas, but few studies have been reported on feature identification monitoring based on deserted steppes [14].

Desert steppes have harsh climatic conditions and extensive degradation areas, and the area of grassland rodent holes is narrow, with a relatively hidden location. In this study, in order to achieve the accurate identification of grassland ratholes in large areas,

based on the advantages of UAVs, a hyperspectral imager was integrated with a UAV to collect the surface spectral information of a desert steppe. With desert steppe ratholes as the research object, relying on the unique spectral characteristics of ratholes, a method of rathole identification based on principal component analysis is proposed, which can quickly and accurately identify desert steppe ratholes with high accuracy. The proposed scientific method provides a technical means for the dynamic monitoring of grassland rodent activity areas and a sound grassland rodent monitoring system. It also contributes to curbing grassland rodent outbreaks at the source and controlling the threat of plague and other infectious diseases to human health.

2. Materials and Methods

2.1. Overview of the Study Area

The experimental area is located in the Gegen Tara grassland (41.78° N, 111.88° E, 1440 m above sea level) in Shiziwangqi, Ulanqab City, Inner Mongolia Autonomous Region (Figure 1). The area is a typical desert steppe environment, with a mid-temperate continental monsoon climate, annual average temperature of 1–6 °C, minimum temperature reaching −39 °C, maximum temperature around 36 °C, annual rainfall around 300 mm, and soil water content of 10.99–13.78%. The soil type is predominantly light chestnut calcium soil with a low vegetation cover and an overall sparse, low performance, mainly dominated by short-flowered needlegrass, cold artemisia, awnless cryptomeria, and camelina [15,16]. The area is a natural source of highland gerbil plague, and common pests include *Meriones unguiculatus*, *Rhombomys opimus*, *Spermophilus dauricus*, *Meriones meridianus pallas*, *Ochotona curzoniae*, *Myospalax psilurus*, *Myospalax aspalax*, *Lasiopodomys brandtii*, and 16 other species [17]. Affected by climatic conditions, rathole openings are relatively small and hidden. Their typical shape is shown in Figure 2. Grassland pest rats start to breed in spring and reach their peak numbers in the summer and autumn; then, the temperature drops, and the mortality rate of pest rats increases until their number reaches the minimum in the following year, with the cycle starting over again. According to surveys, the number of long-clawed gerbils, which are the main host of the plague, has been increasing year by year, and the risk factor for grassland destruction has increased.

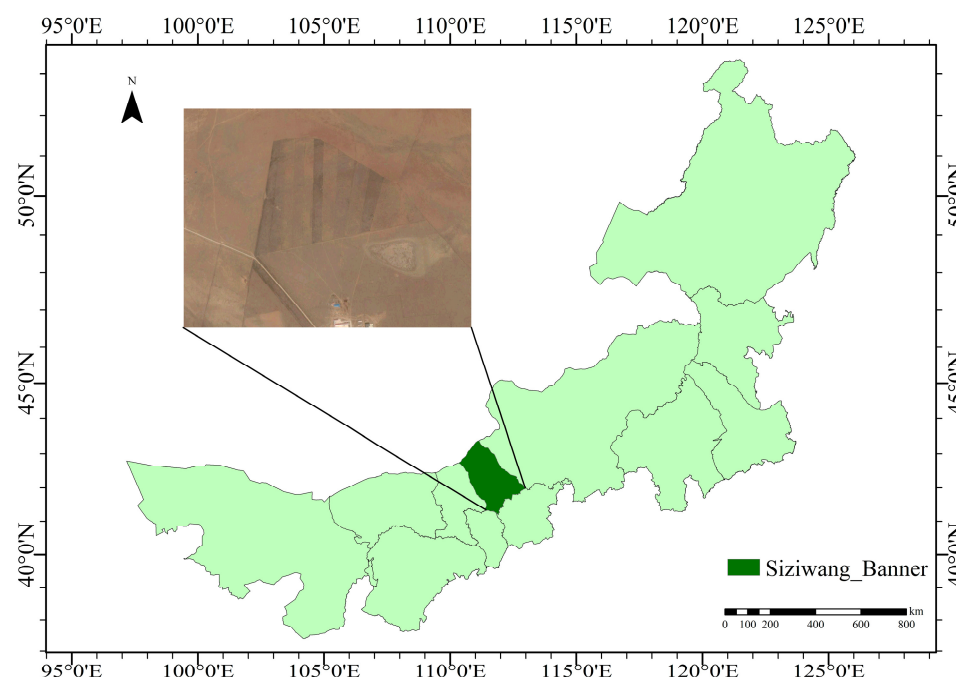


Figure 1. Overview map of the test area.

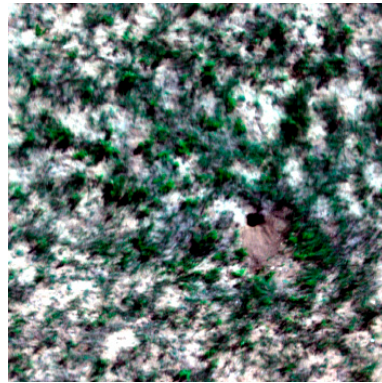


Figure 2. Overview of a rathole.

2.2. Brief Description of the Experimental Equipment

The data collection system used in this study consisted of a DJI Matrice 600 Pro hexacopter drone and a GaiaSky-mini hyperspectral imager (Figure 3). The UAV has its own landing gear, weighs 9.5 kg, has a symmetric motor axis distance of 1133 mm and a maximum takeoff mass of 15.5 kg, and can withstand a maximum wind speed of 5 m/s. The aircraft was equipped with an A3 Pro flight control system and a Lightbridge 2 HD digital image transmission module. The selected hyperspectral imager was a GaiaSky-mini imaging system from Sichuan Shuangli Hopspectrum, with a spectral band range of 400–1000 nm and a spectral resolution of 3.5 nm. The imaging lenses were OL and OLE series lenses (standard configuration: Hsia-OL23), and the photo mode was hovering built-in scanning shooting. The hyperspectral imager and UAV were connected using a DJI RONIN-MX gimbal to ensure smoothness during the data acquisition, thus further guaranteeing the availability of data. The gimbal, spectral imager, and UAV were integrated to remotely control the data acquisition for real-time data visualization.



Figure 3. UAV hyperspectral remote sensing platform.

2.3. Data Acquisition

The data acquisition period was July–August 2019, and the acquisition time was set to 11:00–13:00. To ensure that external environmental interference was minimized during the

data acquisition process, the data were collected under breezy, clear (less cloudy) weather, with a preset UAV flight height of 30 m, a spatial resolution of 2.3 cm, and a data collection area of 2.5 hm². In order to facilitate the subsequent data processing, and to ensure the validity of the data, each party needed to collect data three times.

3. Data Processing

3.1. Data Pre-Processing

The collected raw data were first screened via manual visual inspection, and the overexposed or underexposed data were removed. The remaining spectral images with good shooting results were corrected for reflectance using SpecVIEW (version number 2.9.1.8), which transformed the DN value of the original spectral data into spectral reflectance.

Noise is an unavoidable interference factor in the process of spectral data acquisition. Due to the limitations of the equipment itself, the hyperspectral data acquisition process is affected by the equipment sensor accuracy, dark currents, and the data transmission process, which leads to the contamination of hyperspectral data with various types of noise, including Gaussian noise, streak noise, and impulse noise [18]. The presence of noise will affect the real validity of the spectral data. Therefore, data smoothing and noise reduction are important steps in hyperspectral data processing. In this study, the Savitzky–Golay smoothing filter was selected to smooth and reduce the noise of the spectral data, and the effect of smoothing and noise reduction was achieved without changing the trend of the spectral variation.

3.2. Extraction of Feature Image Elements and Spectral Curve Analysis

After pre-processing, the hyperspectral data need to be extracted from the region of interest. Since the vegetation of desert steppes is interspersed, there is a problem of misclassification of feature image elements due to the fusion of mixed image elements when analyzing the spectral data based on pixels. Therefore, in this study, the pure image elements between different features were extracted from the region of interest, and the pure image elements in the region of interest were selected for spectral averaging. Based on this, the average spectral curve was drawn (Figure 4).

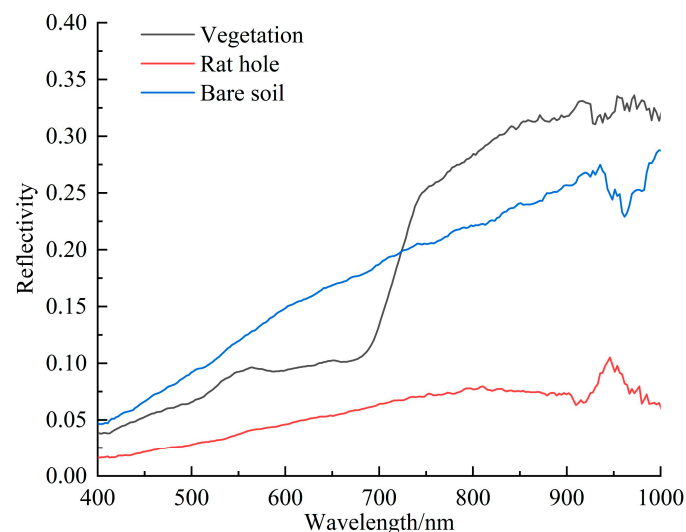


Figure 4. Spectral curve.

It can be seen in Figure 4 that in the visible range, vegetation was affected by chlorophyll and showed a “green peak and red valley” when illuminated by natural light, i.e., the reflectance of the green light band was stronger, and the absorption rate of the red light band was higher, with the highest reflectance reaching 0.35; the spectral reflectance of bare soil showed a positive correlation with the increase in wavelength, and the reflectance of

vegetation was higher than that of bare soil. The spectral reflectance of bare soil increased with the wavelength and was overtaken by that of vegetation after the intersection. The reflectance of vegetation and bare soil in the near-infrared wavelength range increased smoothly with the increase in wavelength. When the low-altitude remote sensing data were collected under the premise of direct sunlight, the background of the rathole showed a black color, and the absorption rate of all wavelengths of natural light was high; thus, the spectral reflectance of the rathole was low.

3.3. Principal Component Analysis

Hyperspectral data have many continuous bands and are high-dimensional data, and the spectral information contains a large amount of useless information. In the process of data analysis, redundant data information will increase the difficulty and time cost of data processing, and reduce its efficiency; therefore, it is necessary to reduce the dimensionality of the spectral data to extract the main spectral characteristic information. Principal component analysis can reduce the dimensionality of the data and minimize the redundant information among different variables by diagonalizing the covariance matrix, so as to compress the multi-band image information to a preset number of bands and achieve the effect of feature extraction. In this study, principal component analysis was performed on 50 spectral samples of each of the three types of features in the 400–700 nm and 400–1000 nm bands.

The corresponding contribution rates and cumulative contribution rates of the first six principal components are presented in Table 1. For the 400–1000 nm band range, the contribution of the first principal component was 77.35%, the cumulative contribution of the first three principal components was 95.81%, and the cumulative contribution of the first six principal components reached 98.16%. For the 400–700 nm band, the contribution of the first principal component was 76.02%, the cumulative contribution of the first three principal components reached 99.07%, and the cumulative contribution of the first six principal components reached 99.59%. From the data in the table, it can be seen that, under the premise of a certain number of principal components, the contribution rate of the spectral data in the range of 400–1000 nm was higher compared with that in the range of 400–700 nm when the spectral data were selected for analysis. Meanwhile, the cumulative contribution rate of the first three principal components reached more than 95%, indicating that the first three principal components could be used to describe most of the features.

Table 1. Corresponding contribution rates and cumulative contribution rates of the first six principal components.

PC Band	400~700 nm		400~1000 nm	
	Contribution Rate	Cumulative Contribution Rate (%)	Contribution Rate	Cumulative Contribution Rate (%)
1	0.7602	76.02	0.7735	77.35
2	0.2211	98.13	0.1581	93.16
3	0.0094	99.07	0.0265	95.81
4	0.0026	99.33	0.0119	97.00
5	0.0014	99.47	0.0066	97.66
6	0.0012	99.59	0.0050	98.16

4. Result

4.1. Rathole Feature Extraction

Hyperspectral images were loaded with RGB images via band reorganization after principal component analysis, and it was found that the image features were more obvious using the combination of the first three principal components, while the spectral images were found to be blurred when the last three principal components were selected for combination, which was not conducive to the subsequent image delineation. To address this problem, in this study, a single principal component was selected for data analysis,

and the single-band hyperspectral data of each of the seven principal components were raster-density-divided based on the DN values of the pixel points (Figure 5). According to the color band variation, the feature extraction results of each principal component in the figure were analyzed, and it was found that the best feature extraction of ratholes was achieved when PC Band1 was selected. The extracted mask image is shown in Figure 6.

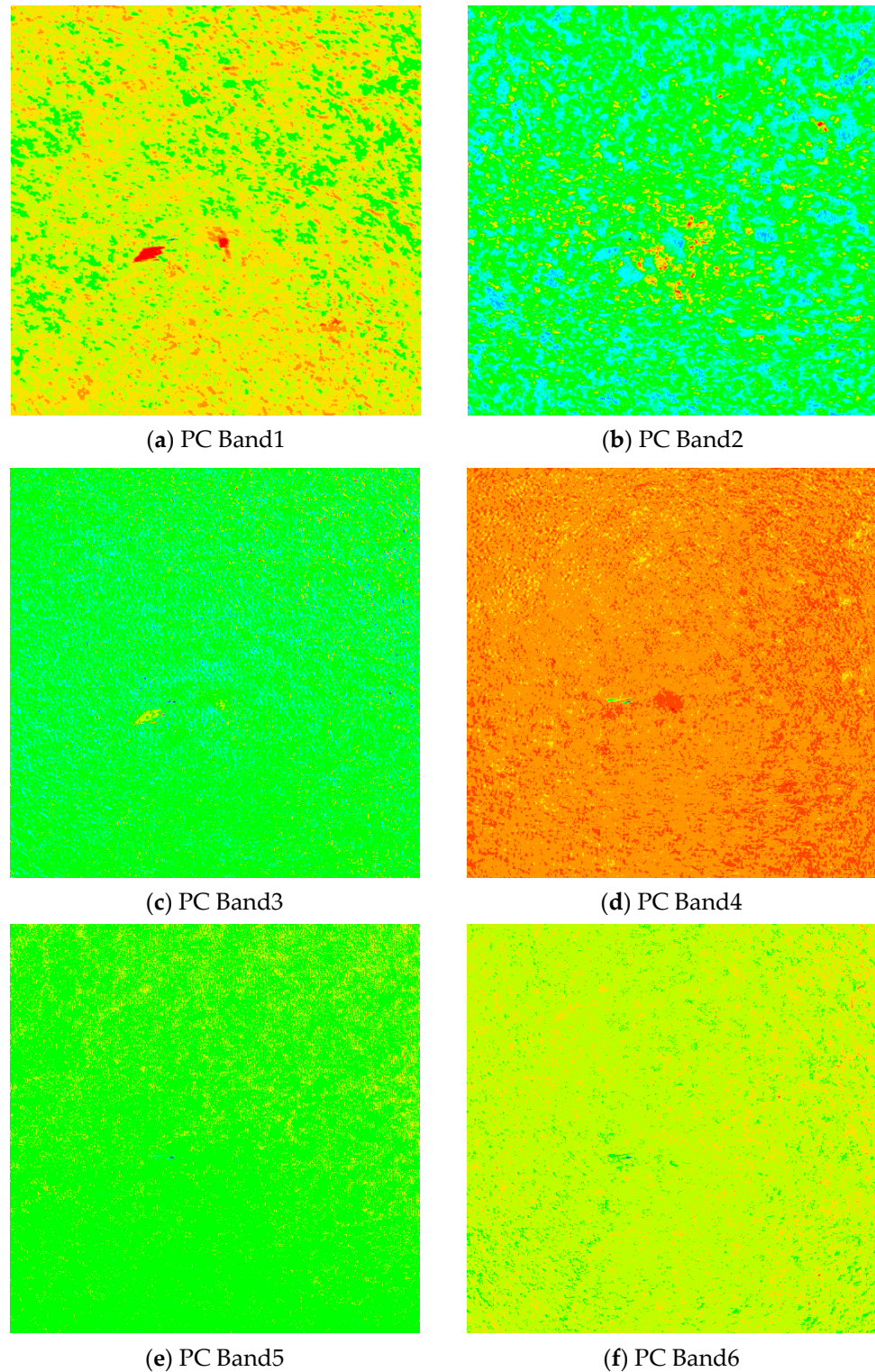


Figure 5. Single-band plot of principal components.



Figure 6. Rathole.

4.2. Non-Rathole Area Characterization

Remote sensing vegetation indices are effective, real-time, empirical measures of surface vegetation conditions, which can indicate the force of vegetation growth and have better sensitivity than single bands used to detect biomass, while the combination of visible and near-infrared bands can effectively obtain various vegetation indices [19]. With the development of technology, there is an extremely strong demand for vegetation indices for applications in agriculture, vegetation, and ecology. Examples include monitoring of vegetation distribution and growth, yield estimation, and extraction of various biological parameters [20]. Common vegetation indices are shown in Table 2.

Table 2. Several common types of vegetation indices.

Vegetation Index	Calculation Formula	References
Normalized difference vegetation index	$NDVI = \frac{(NIR-R)}{(NIR+R)}$	[21,22]
Enhanced vegetation index	$EVI = 2.5 \frac{(NIR-R)}{(NIR+6 \times R-7.5 \times B+1)}$	[23]
Ratio vegetation index	$RVI = \frac{NIR}{R}$	[24]
Difference vegetation index	$DVI = (NIR - R)$	[25]
Soil-adjusted vegetation index	$SAVI = (1 + L) \frac{(NIR-R)}{(NIR+R+L)}$	[26]

NIR stands for near-infrared band; *R* stands for red band; *B* stands for blue band; *L* is the soil conditioning factor, and the value range is 0~1.

The normalized difference vegetation index (NDVI) has the advantages of a wide spatial coverage, high monitoring sensitivity, simple calculation, and effective elimination of radiation interference, which can truly and effectively reflect the vegetation growth state. Moreover, it can be used to calculate the vegetation cover, and is also the most widely used vegetation index for ecological monitoring [27,28]. The normalized vegetation index is more applicable to desert steppes than the other vegetation indices mentioned above because of the sparse vegetation and low vegetation cover. The NDVI was calculated for the non-rathole area, and the results are shown in Figure 7. The results show that the minimum CV value (cursor value) of each type of sample was -0.019260 , and the maximum value was 2.195495 . To avoid errors, $[-0.05, 2.2]$ was used as the threshold range. According to the statistics for the number of image elements and the threshold range after the operation (Table 3), the threshold range of ratholes was $[1.126505, 2.195495]$, the threshold range of bare soil was $[-0.019260, 0.306244]$, and the threshold range of vegetation was $[0.306244, 0.631748]$.

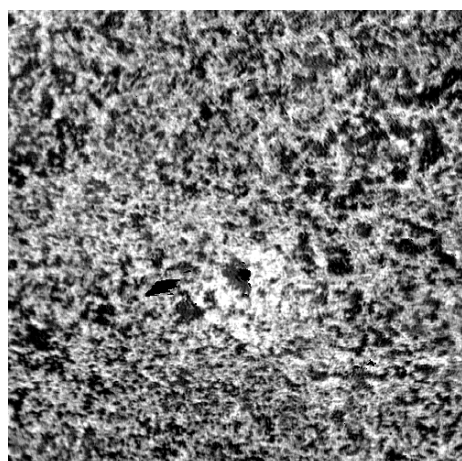


Figure 7. Image of non-rathole area based on NDVI.

4.3. Classification Accuracy Validation

The kappa coefficient is a mathematical calculation based on a confusion matrix to measure the classification accuracy in remote sensing images [29]. In this study, the remaining rathole samples were extracted based on the above method for rathole and non-rathole (vegetation, bare soil) features, and the confusion matrix table based on ratholes and non-ratholes was obtained by creating a mask file and calculating the number of different image elements and threshold statistics, as shown in Table 4. Based on the low-altitude UAV remote sensing platform for rathole data collection, the number of rathole image elements in the sample box was small due to its height, and 347 non-rathole image elements were extracted to improve the accuracy of the precision verification. The overall classification accuracy for the rathole and non-rathole areas reached 97%, and the kappa coefficient reached 0.896. Based on the normalized vegetation index for vegetation, the results of the classification of bare soil and vegetation are shown in Table 3.

Table 3. Color and number of image elements for each type of feature.

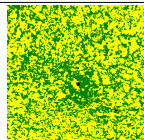
	Color	Name	Number of Pixels	Max Value	Min Value
		Rathole	655	2.195495	1.126505
		Bare soil	148,916	0.306244	−0.019260
		Vegetation	100,429	0.631748	0.306244
	Total		250,000		

Table 4. Confusion matrix of rathole and non-rathole areas.

	Classification Result		
	Rathole	Non-Rathole	Sum
Rathole	143	10	153
Non-rathole	12	335	347
Sum	155	345	500

5. Discussion

Classification methods for hyperspectral images have been proposed by many scholars in their respective research fields, but most of them focus on the feature extraction of single features, such as farmland, buildings, and forests, over large areas. Applying such models to the survey and investigation of small features such as those in desert grasslands will reduce the robustness of the models. This study proposes a new rathole identification model based on a low-altitude UAV hyperspectral remote sensing platform to collect desert steppe rathole spectral data, representing a successful exploration of the application of

low-altitude remote sensing platforms to identify and classify desert steppes and establish early warning mechanisms for grassland rodent damage. Moreover, this study introduces basic research for the subsequent application of this method in large-scale spatial grassland degradation research and grassland rodent damage prevention and control. In the next step, we will apply deep learning technology to spectral data of desert steppe rodent holes and conduct in-depth research on single image elements, soil types, and other factors scattered in the spectral data of desert steppe rodent holes to achieve a more accurate identification and classification. We still need to carry out a lot of experiments and model optimization to conduct in-depth research on grassland degradation and grade evaluation.

6. Conclusions

Grassland ecosystems are an important component of Earth's terrestrial ecosystem, which are tasked with the significant mission of regulating global climate change and precipitation. The need to dynamically monitor grassland degradation and rodent damage is urgent. Currently, the existing vegetation index methods cannot meet the monitoring requirements for desert steppe rodent information and are not effective in extracting rodent hole characteristics in desert steppes. This study collected spectral data of rodent holes in desert steppes using a low-altitude unmanned aerial vehicle hyperspectral remote sensing platform. Based on PCA, the rodent burrow images were extracted, and the threshold interval for the holes was calculated as [1.126505, 2.195495], while the threshold interval for non-burrow areas was [−0.019260, 0.631748]. After validation, the overall classification accuracy reached 97%, and the kappa coefficient reached 0.896. The successful application of this method effectively overcomes the difficulty in identifying rodent holes in desert steppes and improves the identification accuracy. In field surveys of grassland rodent infestation, this method can save labor costs, solve accuracy problems in the identification of fine features based on satellite remote sensing, and, at the same time, enrich the technical means of geospatial data surveys based on low-altitude remote sensing platform application. This method provides a technical means for future research on rodent holes in desert steppes and can provide assistance in monitoring desert steppe degradation, preventing and controlling grassland rodent pests, and preventing plague.

Author Contributions: Conceptualization, J.D. and X.G.; methodology, Y.B. and X.G.; software, X.G.; formal analysis, X.G.; investigation, X.G.; data curation, X.G.; writing—original draft preparation, X.G.; writing—review and editing, J.D. and Y.B.; supervision, J.D. and Y.B.; project administration, J.D.; funding acquisition, J.D. and Y.B. All authors have read and agreed to the published version of the manuscript.

Funding: This research was funded by the National Natural Science Foundation of China, the Key Projects of Higher Education Research in Inner Mongolia Autonomous Region, Natural Science Foundation of Inner Mongolia Autonomous Region Joint Fund Project and Scientific Research Projects of Higher Education Institutions in Inner Mongolia Autonomous Region, grant number No. 31660137, NJZZ23037, 2023LHMS06010 and NJZY21518. The APC was funded by No. 31660137.

Institutional Review Board Statement: Not applicable.

Informed Consent Statement: Not applicable.

Data Availability Statement: Not applicable.

Conflicts of Interest: The authors declare no conflict of interest.

References

1. Pan, Q.; Xue, J.; Tao, J.; Xu, M.; Zhang, W. Current status of grassland degradation and measures for grassland restoration in northern China. *Chin. Sci. Bull.* **2018**, *63*, 1642–1650. [[CrossRef](#)]
2. Guo, B.; Wei, C.; Yu, Y.; Liu, Y.; Li, J.; Meng, C.; Cai, Y. The Dominant Influencing Factors of Desertification Changes in the Source Region of Yellow River: Climate Change or Human Activity? *Sci. Total Environ.* **2022**, *813*, 152512. [[CrossRef](#)] [[PubMed](#)]
3. Li, H.; Li, X.; Yao, Q.; Li, Q. Biolog-ECO analysis of rhizosphere soil microbial community characteristics of five different plants in two different grasslands. *Microbiol. China* **2020**, *47*, 2947–2958. [[CrossRef](#)]

4. Xie, Y.; Wang, Y.; Wu, W.; Guan, Y. Research Progress on Parasites Infection in Rodents. *J. Pathog. Biol.* **2022**, *17*, 1356–1360. [[CrossRef](#)]
5. Feng, Q.; Liu, M.; Bai, Y.; Huang, Y.; Li, Y.; Wang, D.; Shi, W.; Wang, S.; Si, H.; Wang, H. Advances in research on vaccines for rodent-borne diseases. *Chin. J. Vector Biol. Control* **2022**, *33*, 760–764. [[CrossRef](#)]
6. Tang, H.; Gao, W.; Xu, L.; Yan, R.; Chen, B.; Xin, X. Monitoring forage harvesting area in semi-arid pasture based on Landsat TM images. *Trans. Chin. Soc. Agric. Eng.* **2015**, *31*, 160–167. [[CrossRef](#)]
7. Shen, B.; Wei, Y.; Ma, L.; Xu, D.; Ding, L.; Hou, L.; Qin, Q.; Xin, X. Spatiotemporal changes and drivers of fractional vegetation cover in Inner Mongolia grassland of China. *Trans. Chin. Soc. Agric. Eng.* **2022**, *38*, 118–126. [[CrossRef](#)]
8. Lin, Y. A Method for Estimating the Number of Rodents in Grasslands by Estimating Their Orifices. *Chin. J. Zool.* **1975**, *1*, 41–42. [[CrossRef](#)]
9. Hua, R.; Zhou, R.; Bao, D.; Dong, K.; Tang, Z.; Hua, L. A study of UAV remote sensing technology for classifying the level of plateau pika damage to alpine rangeland. *Acta Prataculturae Sin.* **2022**, *31*, 165–176. [[CrossRef](#)]
10. Zumo, I.M.; Hashim, M.; Hassan, N. Mapping Grass above-Ground Biomass of Grazing-Lands Using Satellite Remote Sensing. *Geocarto Int.* **2022**, *37*, 4843–4856. [[CrossRef](#)]
11. Du, R.; Chen, J.; Zhang, Z.; Xu, Y.; Zhang, X.; Yin, H.; Yang, N. Inversing soil salinity under vegetation cover using Sentinel-2 multispectral satellite remote sensing. *Trans. Chin. Soc. Agric. Eng.* **2021**, *37*, 107–115. [[CrossRef](#)]
12. Dutta, S.; Sharma, S.A.; Khera, A.P.; Ajai; Yadav, M.; Hooda, R.S.; Mothikumar, K.E.; Manchanda, M.L. Accuracy Assessment in Cotton Acreage Estimation Using Indian Remote Sensing Satellite Data. *ISPRS J. Photogramm. Remote Sens.* **1994**, *49*, 21–26. [[CrossRef](#)]
13. Wen, A.; Zheng, J.; Chen, M.; Mu, C.; Ma, T. Monitoring Mouse-Hole Density by *Rhombomys opimus* in Desert Forests with UAV Remote Sensing Technology. *Sci. Silvae Sin.* **2018**, *54*, 186–192. [[CrossRef](#)]
14. Du, M.; Noguchi, N.; Itoh, A.; Shibuya, Y. Multi-Temporal Monitoring of Wheat Growth by Using Images from Satellite and Unmanned Aerial Vehicle. *Int. J. Agric. Biol. Eng.* **2017**, *10*, 1–13. [[CrossRef](#)]
15. Zhu, X.; Bi, Y.; Du, J.; Gao, X.; Zhang, T.; Pi, W.; Zhang, Y.; Wang, Y.; Zhang, H. Research on Deep Learning Method Recognition and a Classification Model of Grassland Grass Species Based on Unmanned Aerial Vehicle Hyperspectral Remote Sensing. *Grassl. Sci.* **2023**, *69*, 3–11. [[CrossRef](#)]
16. Pi, W.; Du, J.; Bi, Y.; Gao, X.; Zhu, X. 3D-CNN Based UAV Hyperspectral Imagery for Grassland Degradation Indicator Ground Object Classification Research. *Ecol. Inform.* **2021**, *62*, 101278. [[CrossRef](#)]
17. Xie, X.; Nan, X.; Li, Y.; Li, F.; Liu, B.; Wu, S.; Wang, H. An analysis of the epidemiological characteristics of animal plague in Siziwang banner, Ulanqab, Inner Mongolia, China, 2009–2019. *Chin. J. Vector Biol. Control* **2020**, *31*, 602–606. [[CrossRef](#)]
18. Wang, G.; Han, H.; Carranza, E.J.M.; Guo, S.; Guo, K.; Xiao, K. Tensor-Based Low-Rank and Sparse Prior Information Constraints for Hyperspectral Image Denoising. *IEEE Access* **2020**, *8*, 102935–102946. [[CrossRef](#)]
19. Filla, V.A.; Coelho, A.P.; Bettiol, J.V.T.; Leal, F.T.; Lemos, L.B.; Rosalen, D.L. Model Performance in Estimating the Yield of Common Bean Cultivars. *Rev. Ciência Agronômica* **2023**, *54*, e20217835. [[CrossRef](#)]
20. Wang, M.; Luo, Y.; Zhang, Z.; Xie, Q.; Wu, X.; Ma, X. Recent advances in remote sensing of vegetation phenology: Retrieval algorithm and validation strategy. *Natl. Remote Sens. Bull.* **2022**, *26*, 431–455. [[CrossRef](#)]
21. Liu, H.Q.; Huete, A. A Feedback Based Modification of the NDVI to Minimize Canopy Background and Atmospheric Noise. *IEEE Trans. Geosci. Remote Sens.* **1995**, *33*, 457–465. [[CrossRef](#)]
22. Lichtenhaler, H.K.; Lang, M.; Sowinska, M.; Heisel, F.; Miehe, J.A. Detection of Vegetation Stress via a New High Resolution Fluorescence Imaging System. *J. Plant Physiol.* **1996**, *148*, 599–612. [[CrossRef](#)]
23. Buschmann, C.; Nagel, E. In Vivo Spectroscopy and Internal Optics of Leaves as Basis for Remote Sensing of Vegetation. *Int. J. Remote Sens.* **1993**, *14*, 711–722. [[CrossRef](#)]
24. Wang, H.; Shi, R.; Liu, P.; Gao, W. Dual NDVI Ratio Vegetation Index: A Kind of Vegetation Index Assessing Leaf Carotenoid Content Based on Leaf Optical Properties Model. *Spectrosc. Spectr. Anal.* **2016**, *36*, 2189–2194.
25. Perry, C.R.; Lautenschlager, L.F. Functional Equivalence of Spectral Vegetation Indices. *Remote Sens. Environ.* **1984**, *14*, 169–182. [[CrossRef](#)]
26. Huete, A.R. A Soil-Adjusted Vegetation Index (SAVI). *Remote Sens. Environ.* **1988**, *25*, 295–309. [[CrossRef](#)]
27. Zhang, T.; Du, J.; Zhang, H.; Pi, W.; Gao, X.; Zhu, X. Research on recognition method of desert steppe rat hole based on unmanned aerial vehicle hyperspectral. *J. Optoelectron. Laser* **2022**, *33*, 120–126. [[CrossRef](#)]
28. Marín, J.; Yousfi, S.; Mauri, P.V.; Parra, L.; Lloret, J.; Masaguer, A. RGB Vegetation Indices, NDVI, and Biomass as Indicators to Evaluate C3 and C4 Turfgrass under Different Water Conditions. *Sustainability* **2020**, *12*, 2160. [[CrossRef](#)]
29. Gao, X.; Du, J.; Bi, Y.; Pi, W.; Zhu, X.; Zhang, Y. Spectral Characteristics Analysis and Extraction of Micro-Patches Based on the Hyperspectral Desert Steppe Images. *INMATEH Agric. Eng.* **2022**, *67*, 128–136. [[CrossRef](#)]

Disclaimer/Publisher’s Note: The statements, opinions and data contained in all publications are solely those of the individual author(s) and contributor(s) and not of MDPI and/or the editor(s). MDPI and/or the editor(s) disclaim responsibility for any injury to people or property resulting from any ideas, methods, instructions or products referred to in the content.